Published in final edited form as:
Neuroimage. 2009 April 15; 45(3): 645–655. doi:10.1016/j.neuroimage.2009.01.004.

Alzheimer's Disease Neuroimaging Initiative: A one-year follow up study using tensor-based morphometry correlating degenerative rates, biomarkers and cognition

Alex D. Leow[a,b,*], **Igor Yanovsky**[c], **Neelroop Parikshak**[a], **Xue Hua**[a], **Suh Lee**[a], **Arthur W. Toga**[a], **Clifford R. Jack Jr.**[d], **Matt A. Bernstein**[d], **Paula J. Britson**[d], **Jeffrey L. Gunter**[d], **Chadwick P. Ward**[d], **Bret Borowski**[d], **Leslie M. Shaw**[e], **John Q. Trojanowski**[e], **Adam S. Fleisher**[f], **Danielle Harvey**[g], **John Kornak**[h], **Norbert Schuff**[i], **Gene E. Alexander**[k], **Michael W. Weiner**[i,j], and **Paul M. Thompson**[a] **The Alzheimer's Disease Neuroimaging Initiative**

a *Laboratory of Neuro Imaging, Department of Neurology, UCLA School of Medicine, Los Angeles, CA, USA*

b *Resnick Neuropsychiatric Hospital at UCLA, Los Angeles, CA, USA*

c *Department of Mathematics, University of California, Los Angeles, CA, USA*

d *Mayo Clinic, Rochester, MN, USA*

e *Department Pathology and Laboratory Medicine, and Institute on Aging, University of Pennsylvania School of Medicine, Philadelphia, PA, USA*

f *Department of Neurosciences, UC San Diego, La Jolla, CA, USA*

g *Department of Public Health Sciences, UC Davis School of Medicine, Davis, CA, USA*

h *Department of Radiology and Biomedical Imaging and Department of Epidemiology and Biostatistics, UC San Francisco, San Francisco, CA, USA*

i *Veterans Affairs Medical Center, and Department Radiology, UC San Francisco, San Francisco, CA, USA*

j *Department Medicine and Psychiatry, UC San Francisco, San Francisco, CA, USA*

k *Department Psychology and Evelyn F. McKnight Brain Institute, University of Arizona, Tucson, AZ, USA*

Abstract

Tensor-based morphometry can recover three-dimensional longitudinal brain changes over time by nonlinearly registering baseline to follow-up MRI scans of the same subject. Here, we compared the anatomical distribution of longitudinal brain structural changes, over 12 months, using a subset of the ADNI dataset consisting of 20 patients with Alzheimer's disease (AD), 40 healthy elderly controls, and 40 individuals with mild cognitive impairment (MCI). Each individual longitudinal change map (Jacobian map) was created using an unbiased registration technique, and spatially normalized to a geometrically-centered average image based on healthy controls. Voxelwise statistical analyses revealed regional differences in atrophy rates, and these differences were correlated with clinical measures and biomarkers. Consistent with prior studies, we detected widespread cerebral atrophy in AD, and a more restricted atrophic pattern in MCI. In MCI, temporal lobe atrophy rates were correlated with changes in mini-mental state exam (MMSE) scores, clinical dementia rating (CDR), and logical/verbal learning memory scores. In AD, temporal atrophy rates

*Corresponding author. Laboratory of Neuro Imaging, Department of Neurology, UCLA School of Medicine, Neuroscience Research Building 225E, 635 Charles Young Drive, Los Angeles, CA 90095-1769, USA. Fax: +1 310 206-5518. E-mail address: E-mail: feuillet@ucla.edu (A.D. Leow).

were correlated with several biomarker indices, including a higher CSF level of p-tau protein, and a greater CSF tau/beta amyloid 1-42 (ABeta42) ratio. Temporal lobe atrophy was significantly faster in MCI subjects who converted to AD than in non-converters. Serial MRI scans can therefore be analyzed with nonlinear image registration to relate ongoing neurodegeneration to a variety of pathological biomarkers, cognitive changes, and conversion from MCI to AD, tracking disease progression in 3-dimensional detail.

Introduction

Alzheimer's disease is the most common form of dementia, afflicting over 24 million people worldwide. In early AD, short-term memory function is typically among the first to be impaired, followed by a progressive decline in other cognitive functions (such as language, attention, orientation, visuospatial skills, and executive function) along with emotional/behavioral disturbances. At present, there is no cure for AD, whose natural course is insidious yet gradually debilitating, and is typically fatal at its most advanced stage, usually due to medical complications. In recent years, scientific interest has also focused on mild cognitive impairment (MCI), a pre-dementia stage that carries a 4–6-fold increased risk of future diagnosis of dementia, relative to the general population (Petersen et al., 1999, 2001; Petersen, 2000).

Many investigators have used MRI and PET imaging to measure longitudinal progression of brain changes in normal aging, MCI and AD, with varying results. As drug candidates that might slow the progression of Alzheimer's pathology began to be developed, the need to develop robust and sensitive imaging methods to quantify progression of Alzheimer's disease has become increasingly important. To this end, the National Institute of Aging and pharmaceutical industry funded the Alzheimer's Disease Neuroimaging Initiative, with the goal of developing improved methods based on imaging and other biomarkers, for AD treatment trials.

A variety of methods have been used to quantify the longitudinal changes in structural brain MRI including: region-of-interest measurements (especially of the hippocampus (Frisoni et al., 1999), the "boundary shift integral" technique which quantifies differences between two successive co-registered 3D MRIs (Fox et al., 2000), voxel-based morphometry (Good et al., 2001; Whitwell et al., 2007), and tensor-based morphometry (Studholme et al., 2004, 2006; Leow et al., 2007).

Tensor-based morphometry (TBM) is a relatively new image analysis technique that identifies regional structural differences in the brain, across groups or over time, from the gradients of the deformation fields that align, or 'warp,' images to a common anatomical template (reviewed in Ashburner and Friston, 2003). Highly automated methods such as TBM are being tested to examine their utility in large-scale clinical trials, and in studies to identify factors that influence disease onset and progression (Leow et al., 2005b; Cardenas et al., 2007), or normal development (Thompson et al., 2000a; Chung et al., 2001; Hua et al., 2007).

In this paper, TBM is applied to a longitudinal ADNI dataset by using a nonlinear registration algorithm to match 3D baseline structural MR images with follow-up images acquired 1 year later (for related approaches, see Leow et al. 2005a; Studholme et al., 2006; Studholme and Cardenas, 2007; van de Pol et al., 2007; Barnes et al., 2008; Ridha et al., 2008).

Color-coded Jacobian maps — which show the local expansion or compression factor at each point in the image — can be used to indicate local volume loss or gain relative to the baseline image (Freeborough and Fox, 1998; Chung et al., 2001; Fox et al., 2001; Ashburner and Friston, 2003; Riddle et al., 2004). Here we examined longitudinal brain changes, using these Jacobian

maps, in groups of AD and MCI subjects relative to controls. We also investigated, at a voxelwise level, how ongoing brain atrophy correlated with clinical measures including MMSE scores, and the global Clinical Dementia Rating (CDR), as well as biomarkers of AD pathology including CSF levels of tau protein, 181-phosphorylated tau protein (p-tau), beta amyloid (ABeta 42), and tau/Abeta42 ratio (Andreasen et al. 2001; Itoh et al., 2001; Verbeek et al., 2003; Clark et al., 2003; Hampel et al., 2004; Lee and Trojanowski, 2006).

Our hypotheses were as follows: (1) brain atrophic rates would be greater in AD and MCI than in controls, with MCI-control differences restricted primarily to the temporal lobe; (2) MCI converters (who transitioned to AD during the one-year follow-up interval) would have faster atrophic rates than non-converters, but slower atrophic rates than those with AD; (3) longitudinal temporal lobe atrophy would be significantly correlated with progression of cognitive impairment in AD and MCI; and (4) higher CSF tau protein level, lower CSF ABeta42 level, and higher p-tau/ABeta42 ratio would be significantly associated with higher rates of temporal lobe atrophy. In further tests that were considered exploratory rather than hypothesis-based, for purposes of statistical inference, we also determined which additional CSF biomarkers might correlate best with atrophic rates in each diagnostic group, and in all subjects combined.

Methods

Subjects

The Alzheimer's Disease Neuroimaging Initiative (ADNI) (Mueller et al., 2005a,b) is a large multi-center longitudinal MRI and FDG-PET (fluorodeoxyglucose positron emission tomography) study of 800 adults, ages 55 to 90, including 200 elderly controls, 400 MCI subjects, and 200 AD patients. The ADNI was launched in 2003 by the National Institute on Aging (NIA), the National Institute of Biomedical Imaging and Bioengineering (NIBIB), the Food and Drug Administration (FDA), private pharmaceutical companies and non-profit organizations, as a $60 million, 5-year public–private partnership. The primary goal of ADNI has been to test whether serial MRI, PET, other biological markers, and clinical and neuropsychological assessments acquired in a multi-site manner mirroring enrollment methods used in clinical trials, can replicate results from smaller single site studies measuring the progression of MCI and early AD. Determination of sensitive and specific markers of very early AD progression is intended to aid researchers and clinicians to develop new treatments and monitor their effectiveness, as well as lessen the time and cost of clinical trials.

At the time of writing this report, data collection for the ADNI project was in progress. In this paper, we studied longitudinal brain structural changes in 100 subjects, divided into 3 groups: 40 healthy elderly individuals, 40 individuals with amnestic MCI, and 20 individuals with probable AD. All groups were well matched for gender and age: each group included 50% men and 50% women; mean ages for the control, MCI and AD groups were, respectively, 75.27 years (standard deviation (SD)=5.33 years), 75.43 years (SD=7.02), and 75.70 years (SD=7.36), with no significant age differences among the three groups. We included twice as many subjects in the MCI and control groups versus the AD group, based on the availability of one-year follow-up scans at the time of writing this paper.

All subjects underwent thorough clinical/cognitive assessment at the time of both the baseline and the follow-up scan acquisitions. As part of each subject's cognitive evaluation, the Mini-Mental State Examination (MMSE) was administered to provide a global measure of mental status based on evaluation of five cognitive domains (Folstein et al., 1975; Cockrell and Folstein, 1988); scores of 24 or less (out of a maximum of 30) are generally consistent with dementia. The Clinical Dementia Rating (CDR) was also assessed as a measure of dementia severity (Hughes et al., 1982; Morris, 1993). A global CDR of 0, 0.5, 1, 2 and 3, respectively,

indicate no dementia, very mild, mild, moderate, and severe dementia. The elderly normal subjects had MMSE scores between 28 and 30 (inclusive), all had a global CDR of 0, and no symptoms of depression, MCI, or other forms of dementia. The MCI subjects had MMSE scores in the range of 24 to 30, all had a global CDR of 0.5, and mild memory complaints, with memory impairment assessed via education-adjusted scores on the Wechsler Memory Scale–Logical Memory II (Wechsler, 1987). All AD patients met NINCDS/ADRDA criteria for probable AD (McKhann et al., 1984) with baseline MMSE scores as high as 26, and a lower limit of 20. In this study, 16 AD patients had a CDR of 0.5, and the remainder had a CDR of 1. Detailed exclusion criteria, e.g., regarding concurrent use of psychotropic medications, can be found in the ADNI protocol (Mueller et al., 2005a,b). Briefly, subjects were excluded if they had any serious neurological disease other than incipient AD, any history of brain lesions or head trauma, or psychotropic medication use (including antidepressants, neuroleptics, chronic anxiolytics or sedative hypnotics, etc.).

MRI acquisition and image correction

All subjects were scanned with a standardized MRI protocol, developed after a substantial effort evaluating and comparing 3D T1-weighted sequences for morphometric analyses (Leow et al., 2006; Jack et al., 2008). High-resolution structural brain MRI scans were acquired at multiple ADNI sites using 1.5 Tesla MRI scanners from General Electric Healthcare and Siemens Medical Solutions (ADNI also collects a smaller subset of data at 3 Tesla but it was not analyzed here to avoid the additional complications of combining data across scanner field strengths). All scans were collected according to the standard ADNI MRI protocol. For each subject, two T1-weighted MRI scans were collected using a sagittal 3D MP-RAGE sequence. As described in Jack et al. (2008), typical 1.5 T acquisition parameters are repetition time (TR) of 2400 ms, minimum full TE, inversion time (TI) of 1000 ms, flip angle of 8°, 24 cm field of view, with a 192×192×166 acquisition matrix in the *x*-, *y*-, and *z*-dimensions yielding a voxel size of 1.25×1.25×1.2 mm^3. In-plane, zero-filled reconstruction yielded a 256×256 matrix for a reconstructed voxel size of 0.9375× 0.9375×1.2 mm^3.

Additional image corrections were also applied, using a processing pipeline at the Mayo Clinic, consisting of: (1) a procedure termed *GradWarp* for correction of geometric distortion due to gradient non-linearity (Jovicich et al., 2006), (2) a “B1-correction,” to adjust for image intensity inhomogeneity due to B1 non-uniformity using calibration scans (Jack et al., 2008), (3) “N3” bias field correction, for reducing residual intensity inhomogeneity (Sled et al., 1998), and (4) geometrical scaling, according to a phantom scan acquired for each subject (Jack et al., 2008), to adjust for scanner- and session-specific calibration errors. In addition to the original uncorrected image files, images with all of these corrections already applied (GradWarp, B1, phantom scaling, and N3) are available to the general scientific community (at www.loni.ucla.edu/ADNI).

Image pre-processing

To adjust for global differences in brain positioning and scale across individuals, all scans were linearly registered to the stereotactic space defined by the International Consortium for Brain Mapping (ICBM-53) (Mazziotta et al., 2001) with a 9-parameter (9P) transformation (3 translations, 3 rotations, 3 scales) using the Minctracc algorithm (Collins et al., 1994). Globally aligned images were resampled in an isotropic space of 220 voxels along each axis (*x*, *y*, and *z*) with a final voxel size of 1 mm^3.

Specifically, baseline scans were first linearly normalized with a 9-parameter registration to the ICBM space. Follow-up scans, on the other hand, were 9-parameter registered to their corresponding baseline scans, followed by normalization to the ICBM space using the same

baseline transformation that carries baseline scans to the ICBM space (for discussions on the effect of global scaling in longitudinal studies, see Paling et al., 2004; Whitwell et al., 2004).

Three-dimensional Jacobian maps quantifying structural changes over time

To quantify 3D patterns of volumetric brain atrophy over time for each subject, an individual change map, or Jacobian map, was computed by non-linearly registering the follow-up scan to the baseline scan with an unbiased registration algorithm we developed (Leow et al., 2007). The unbiased image registration technique computes deformation fields by penalizing statistical bias in the resulting Jacobian maps, thus eliminating skew from the distribution of Jacobian determinants, and has been shown to perform favorably in recovering true physiological changes in serial MRI data (Yanovsky et al., 2007). Non-positive Jacobians are prevented when using unbiased registration, as a regularization term is penalized based on the logarithmic transform of the local Jacobian values. Moreover, unbiased registration is inherently symmetric (i.e., inverse-consistent), so there is no methodologically-induced bias towards detecting gain versus loss (see Leow et al., 2005, Leow et al., 2007, for examination of the Jacobian statistical distributions).

Unbiased group average template — Minimal Deformation Target (MDT)

To facilitate voxelwise comparisons between groups, we followed our previous approaches and further nonlinearly registered all individual brains and their corresponding Jacobian maps to the Minimal Deformation Target (MDT) created in Hua et al. (2008), an unbiased average template image in the ICBM space representing common anatomical features on a voxel level for the group of control ADNI subjects (Good et al., 2001; Kochunov et al., 2002; Joshi et al., 2004; Studholme and Cardenas, 2004; Kovacevic et al., 2005; Christensen et al., 2006; Lorenzen et al., 2006; Lepore et al., 2008).

After this final step, these spatially normalized Jacobian maps now share a common anatomical coordinate as defined by the MDT. Thus, statistical analyses may be conducted at each voxel to assess the magnitude and significance of deficits in MCI and AD versus the healthy controls.

Statistical tests

Using these spatially normalized Jacobian maps that encode longitudinal brain changes, we carried out voxel-wise statistical tests between the Jacobian maps in each group. The Jacobian maps in MCI and AD were compared to those from normal controls, using both a spatial average of the Jacobian values within specific regions of interest (ROIs; defined below), and voxel-wise tests controlled for multiple comparisons. In the latter, at each voxel, we evaluated the significance level of group differences using a two-sample *t* test with unequal variance. The resulting *p*-values were displayed as maps to visualize patterns of significant differences throughout the brain.

To correct for multiple comparisons, we used permutation testing to assess the overall significance of group differences (see, e.g., Bullmore et al., 1999; Nichols and Holmes 2002; Thompson et al. 2003a,b; Chiang et al., 2007a,b). A null distribution for the group differences in Jacobian at each voxel was constructed using 10,000 random permutations of the data. The number of permutations N was chosen to be 10,000, to control the standard error SEp of the omnibus probability p, which follows a binomial distribution B(N, p) with known standard error (Edgington, 1995). When N=10,000, the approximate margin of error (95% confidence interval) for p is approximately 5% of p. For each test, the subjects' diagnosis was randomly permuted and voxel-wise *t* tests were conducted to identify voxels more significant than p=0.05. The volume of voxels in the brain more significant than p=0.05 was computed for the real experiment and for the random assignments. Finally, a ratio, describing the fraction of the

time the suprathreshold volume was greater in the randomized maps than the real effect (the original labeling), was calculated to give an overall *p*-value for the significance of the map.

CDF plots

Cumulative distribution function (CDF) plots based on the above two-sample *t*-tests were used to compare the effect sizes of group differences and effects of covariates of interest in all three groups. These CDF plots are commonly generated when using false discovery rate methods to assign overall significance values to statistical maps (Benjamini and Hochberg, 1995; Genovese et al., 2002; Storey, 2002); they may also be used to compare effect sizes of different methods, subject to certain caveats (Lepore et al., 2008; Hua et al., 2008; Morra et al., 2008a,b), as they show the proportion of supra-threshold voxels in a statistical map, for a range of thresholds.

Regions of interest (ROIs)

Regions of interest, including frontal, parietal, temporal, and occipital lobes, were defined by manually labeling the normal group MDT. The MDT was traced by a trained anatomist to generate binary masks for each lobe, which were subsequently used to summarize brain atrophy at a regional level in each group. Within each lobe, tissue types were distinguished by creating maps of gray and white matter, CSF, and non-brain tissues using the partial volume classification (PVC) algorithm from the *BrainSuite* software package (Shattuck and Leahy, 2002). One single voxel was eroded from the boundary of each tissue class to avoid the inclusion of partial volumed voxels at tissue interfaces (e.g., CSF, gray and white matter mixtures) where the Jacobian values may not be representative of the rest of the region. To avoid confounding the average values in regions where tissue atrophy was assessed, CSF was excluded from the masks for the ROI-based Jacobian averages, but was included for voxel-wise comparisons (i.e., maps of group differences).

Correlations of structural brain differences (Jacobian values) with clinical measurements and biomarkers

At each voxel, correlations were assessed for each group, using the general linear model, between the Jacobian values and several clinical measures at baseline — MMSE scores (Folstein et al., 1975), the geriatric depression scale (GDS), Clinical Dementia Rating summary scores (Morris, 1993), and CDR sum-of-boxes scores. The CDR assesses a patient's cognitive and functional performance in six areas on a scale of 0 (no impairment) to 3 (impaired): memory, orientation, judgment and problem solving, community affairs, home and hobbies, and personal care. As there is a significant range restriction with global CDR scores, we also assessed correlations with the CDR 'sum-of-boxes' scores, which has a greater dynamic range (0–18), and may provide more useful information than the CDR global score, especially in mild cases (Lynch et al., 2006). In addition, several biomarkers obtained from CSF were also included for assessing correlations, including beta amyloid 1-42 (ABeta42), tau protein, phosphorylated-tau protein 181 (p-tau), the tau and ABeta42 ratio (tau/ABeta42), and p-tau ABeta42 ratio (p-tau/ABeta42). Biomarker measurements were performed by Drs. Leslie Shaw and John Trojanowski of the ADNI Biomarker Core at the University of Pennsylvania School of Medicine, which collects and banks biological samples (DNA, blood, urine and CSF) from all participating sites, and conducts studies of selected AD biomarkers, including apolipoprotein E (ApoE) genotype, isoprostanes, tau, ABeta, and homocysteine levels (Shaw et al., 2007).

As individual Jacobian maps encode structural differences between baseline and follow-up scans, correlations were also assessed between the Jacobian values and the differences in clinical measures between the two time points. All correlations were corrected for multiple comparisons as described above.

Results

3D maps of brain atrophy in MCI and AD

We first visualized the mean brain structural change map for each group (AD, MCI, and CTL) by averaging individual Jacobian maps within each group. These maps may be considered as showing the mean percent tissue loss over the one-year interval, or, if changes are assumed to be approximately linear, they provide a regional estimate of the atrophy rate. The resulting statistical maps, shown in Fig. 1, suggest widespread progressive atrophy throughout the entire brain and expansion of ventricular and CSF spaces in AD (compared to controls), and a more restricted pattern of atrophy in MCI. To test whether there were statistically significant volume changes, over this 12-month time period, for each group, and whether these changes differ between groups, we conducted regional (ROI) analyses as well as voxel-wise tests controlled for multiple comparisons as follows (Figs. 2 and 3).

Mean Jacobian values within each ROI, normalized to indicate annualized rates of atrophy (in percent per year) were computed to represent overall differences in the rates of atrophy for each region (Fig. 3). Here, we also separated MCI converters (N=7) from MCI non-converters (N=32). (These MCI subgroups excluded the one MCI subject whose diagnosis was changed to control at follow-up). In general, a consistent trend was observed for atrophy rates, with AD >MCI converters >MCI non-converters. MCI non-converters showed comparable rates to controls (see bars colored *camel* and *white*, respectively, in Fig. 3). The AD group (N=40) showed significant progressive atrophy (p values, based on 1-sample t-test, <0.01 for all ROIs) in the frontal lobes (annual atrophy rate in AD: 2.41%), occipital lobes (2.07%), parietal lobes (2.40%), and temporal lobes (2.22%). The corresponding mean atrophy rates were 0.37%, 0.63%, 0.22%, and 0.74% for the control group, with corresponding P-values exhibiting significance for the occipital lobes (p=0.02) and the temporal lobes (p=0.05) (the MCI non-converter group showed a similar atrophy profile; see Fig. 3 for more explanations). The small group of MCI converters (N=7) showed an atrophy profile resembling AD (no statistical tests were conducted in this sub-group due to a smaller sample size, although the MCI converters/AD combined group, with a sample size of 27, also exhibited significant volume loss for all ROIs). These data are consistent with earlier reports assessing atrophy rates using 2 MRI brain scans separated by a 12-month interval: using the boundary shift integral method, Fox et al. (2000) found that mean (SD) rate of brain atrophy for the patients with mild to moderate AD was 2.37% (1.11%) per year, while in the control group it was 0.41% (0.47%) per year.

Permutation tests, using suprathreshold percentages, were conducted to assess the presence of statistically significant local volume change differences between groups, based on the voxel-wise two-sample t-test on the rates of change (Fig. 2). This step provides a detailed 3-D visualization of the local atrophy profile, in terms of voxel-wise mean change rates and their significance level). Here, significantly greater atrophy rates in AD versus controls were confirmed for all ROIs, including left/right/both temporal lobes (p=0.0021/0.0015/0.0015, corrected), occipital lobes (p=0.0014, corrected), parietal lobes (p =0.0015, corrected), and frontal lobes (p=0.005, corrected). Also, significantly greater atrophy rates in MCI versus controls were confirmed in the left/right/total temporal lobe (p=0.03/0.03/0.03, corrected), and parietal lobe (p=0.046, corrected) but not in the occipital or frontal lobes (non-converters were not separated in this permutation testing, due to a relatively small sample size of 7). This is consistent with previous findings that parietal and temporal lobes are among the first to be involved in AD. Although mean Jacobian values (Fig. 3) — when spatially averaged across the temporal lobe — were similar in MCI (both converters and non-converters) and controls (annual atrophy rate 0.73% and 0.74%), locally faster atrophy was detected in the MCI group versus controls using a voxelwise permutation test. This is partly due to contributions from the converters, who have smaller Jacobian values in general —denoting faster atrophy — compared to non-converters. This also shows that permutation testing, on the suprathreshold

volume of statistics in a map may be more powerful for detecting group differences than performing univariate tests on regional averages (numeric summaries) derived from the maps.

Correlations of Jacobian values with clinical measures and biomarkers

Any quantitative measure of brain atrophy has greater value if it can be shown to correlate with established measures of cognitive or clinical decline, or with future outcome measures. Here, we investigated whether longitudinal temporal lobe atrophy over this 12-month period correlates with cognitive decline over the same interval. Our results in Tables 1 and 2 show corrected *p*-values for these correlations (although all markers and clinical measures were correlated for each diagnostic group, only significant results are reported here). To avoid reductions in power due to restricting the range to the AD or MCI groups separately, correlations were also examined across the entire sample of 100 subjects (which we will refer to as the "pooled" group). In this case, the normal subjects, who tend to score in the normal range for all clinical measures, drive these associations to some extent. Diagnostic groups were not pooled together for these cognitive tests since the groups are stratified according to their test scores.

Our results in Table 1 and Fig. 4a indicate that higher CSF tau protein level, lower CSF ABeta42 level, and higher p-tau/ABeta42 ratio are significantly associated with higher rates of temporal lobe atrophy only in the pooled group (p=0.003, 0.001 and 0.002, *corrected*), but not in any of the 3 individual diagnostic groups. On the other hand, correlations between temporal lobe atrophy rates and the CSF p-tau level and tau/Abeta42 ratio were significant for both the pooled data (p=0.01 and 0.0003) and within the AD group (p=0.02 and 0.02).

For clinical measures (Table 2; Fig. 4b), longitudinal temporal lobe atrophy was significantly correlated with progression of cognitive impairment in the MCI group, including an increase over time in CDR score (p=0.03), a decrease over time in MMSE (p=0.02), a worsening in immediate logical memory performance (p=0.04), and worsening scores on the 30-minute delayed auditory verbal learning test (AVLT) (p=0.04). Moreover, a higher baseline Geriatric Depression Score (i.e., more severe depression) and a lower baseline score on the delayed logical memory test also correlated with a greater ongoing rate of temporal lobe atrophy (p=0.02 and 0.04). Lastly, converters exhibited significantly faster rates of temporal lobe atrophy (p=0.03) than non-converters (i.e., atrophy rates differentiated the group of converters from non-converters).

Interestingly, in our analysis, longitudinal temporal lobe atrophy was not correlated with baseline MMSE, CDR, or sum-of boxes scores. Nor does it correlate with the change in sum-of-boxes scores over the one-year interval. However, in the AD group, a higher baseline sum-of-boxes score, i.e., greater cognitive impairment at baseline, correlated with less ongoing atrophy (i.e., larger Jacobian values) (p=0.02). In AD, the sum-of-boxes score may therefore better reflect the disease severity in advanced AD, at a point when advanced temporal atrophy has already occurred, and progressive atrophy has slowed.

CDF curves

The cumulative distribution curves in Fig. 4 show relative effect sizes for the associations between rates of brain atrophy and different pathological markers and clinical correlates. In general, curves that rise more sharply at the origin denote statistical maps with greater effect sizes, and those curves that intersect the line $y=20x$ at points other than the origin, pass the conventional criterion of controlling the false discovery rate at an expected rate of 5%, and are regarded as significant after multiple comparisons correction. This approach allows an approximate ranking of the effect sizes for different correlates: higher tau/ABeta42 ratio was the pathological biomarker most highly correlated with higher rates of temporal lobe atrophy

when all subjects were combined; other biomarkers showed comparable but slightly lower effect sizes. The clinical score that correlated most with higher rates of temporal lobe atrophy was one-year change in MMSE in MCI, with many other cognitive measures showing comparable but slightly lower effect sizes.

Discussion

In this paper, our hypotheses were largely confirmed regarding longitudinal brain structural changes in three groups of subjects including normal controls, those with MCI, and patients with Alzheimer's disease. Alzheimer's disease was associated with significantly faster ongoing atrophy in the temporal and parietal lobes, relative to matched healthy controls. There was also significantly faster expansion in the CSF spaces, consistent with previous studies (e.g., Boyes et al., 2006), and significant progressive tissue loss in frontal and occipital lobes, indicating that ongoing atrophy is widely distributed in AD.

Prior studies of the disease trajectory in AD (e.g., Scahill et al., 2002; Thompson et al., 2003a,b), show a shift in the distribution of atrophy with advancing disease. In line with the trajectory of neurofibrillary pathology (Braak and Braak, 1991), the entorhinal and medial temporal lobes show the earliest signs of atrophy in MCI, with frontal atrophy typically occurring later, and primary sensory and motor cortices spared until late in the illness (see Thompson and Apostolova, 2007, for a review of this trajectory mapped with different imaging modalities). Consistent with this, in our MCI group, progressive atrophy was detected only in the temporal and parietal lobes, in line with evidence that ongoing changes are more anatomically restricted at this pre-dementia stage.

One notable aspect of the topography of brain matter loss shown in Figs. 1 and 2 is that the greatest proportion of brain matter loss appears to lie in the white matter rather than at the voxels on the cortical surface. There are two reasons for this, both technical: (1) the deformations are spatially smooth and partial volume averaging effects occur and diminish the signal somewhat at tissue boundaries, such as the cortex/CSF interface, and (2) the registration accuracy of TBM is poorer at the cortical surface, at least relative to some approaches that explicitly model the cortical surface. To clarify this, note that Figs. 1 and 2 visualize group differences by averaging rates of volumetric changes (i.e., Jacobian maps), after nonlinearly aligning individual maps of change to the minimal deformation template (MDT). This deformation field is spatially smooth, so some partial volume effects between cortex and CSF are inevitable and are more pronounced along the MDT boundary. As a result, some signal spillover from outside of the brain tissue may be present, explaining the reduction in the atrophy signal along the boundary. This effect has been noted in our prior work (Hua et al., 2008), where the disease-related expansion in the ventricles spills over into the subcortical white matter by about 1–2 mm, in the average maps. Similarly, the cortical atrophy signal is partially canceled by the signal in the CSF outside the brain, which may not show the same level of atrophy, and if anything, may show slight expansion over time. Second, and perhaps more importantly, the deformation fields are based on automated matching of intensities in the images, and the spatial smoothness of the fields makes it difficult to register the entire cortical mantle within subjects from one time-point to the next, as would be required to gauge the atrophy of cortical gray matter. Alternative approaches may be used that compute thickness at each point, but these are typically more time-consuming as they generally require extraction of explicit models of the cortical surface as geometric meshes, prior to computing the cortical thickness either directly from the meshes (Lerch and Evans, 2005), or by tissue classification of the images and voxel coding (Thompson et al., 2004;Aganj et al., 2008).

There are at least two possible solutions to better sensitizing our TBM approach for detecting cortical gray matter loss. The first is to use a method termed voxel-based morphometry (VBM;

Ashburner and Friston, 2000) or a related approach termed RAVENS (Davatzikos et al., 2001). In VBM, the deformation-based compression signal at each point is multiplied by maps of gray matter density, which are based on smoothing maps of gray matter voxels derived from an explicit tissue classification into gray and white matter and CSF. An additional modulation step is also included that preserves information on the volume of gray matter in the baseline images after warping. When gray matter density and deformation signals are multiplied together in this way, VBM maps in AD do typically show progressive cortical gray matter atrophy in a temporal-to-frontal pattern that matches the spread of neurofibrillary tangle pathology (Baron et al., 2001). A second approach to identifying cortical gray matter atrophy with TBM was developed by (Studholme et al., 2003), in which deformation-based compression signals at each point are smoothed adaptively depending on the amount of gray matter lying under the filter kernel. This is a way to avoid some of the signal depletion that occurs when atrophying gray matter is partial-volumed with CSF. A third solution is to run the deformation maps at a very high spatial resolution and with less spatial regularization, or with a regularization term that enforces continuity but not smoothness. Because of the complexity of differentiating cortical gray matter changes from underlying white matter changes, we seek to assign signals to the cortex without surface-based modeling, which can be time consuming for larger analyses (Thompson et al., 2004), Thus, in this paper, we decided to combine both gray and white matter for each region of interest (ROI) in our analyses, instead of separating them.

Although much of the literature has suggested that gray matter loss is the primary change in AD that is observable on MRI (see Thompson and Apostolova, 2007, for a review), there has been substantial theoretical and empirical evidence supporting white matter pathology in AD (Bartzokis et al., 2003). For example, in Rose et al. (2000), the authors summarized recent DTI studies in AD, and many have reported reduced FA (fractional anisotropy) in temporal, frontal, and parietal lobes, especially in the internal capsule and limbic association fibers, the corticothalamic pathway, superior longitudinal fasciculus, and posterior cingulate bundle (Yoshiura et al., 2002). White matter degeneration in AD has also been detected with MR relaxometry (Bartzokis et al., 2003) and myelin and oligodendrocyte reductions have been detected in neuropathological studies of AD. Future MRI studies, using state-of-the-art techniques such as diffusion-weighted MRI (Rose et al., 2000; Choi et al., 2005; Medina et al., 2006) or High Angular Resolution Diffusion Imaging (HARDI), are likely to further elucidate white matter pathology in AD.

A further notable feature, which requires some explanation, is that a related technique (the voxel-compression method) has shown unequivocally temporal gray matter loss and ventricular expansion, but no change in the white matter (Fox et al., 2001) in serial MRI studies of AD. As already noted, we did indeed detect subtle and diffuse changes in the subcortical white matter, but the ability to detect them depends to some degree on the level of regularization used in TBM. In TBM, there is a smoothness term, which causes correlations in the deformation signals at neighboring voxels. In general, for simplicity and practicality, an elastic (Leow et al., 2005a) or fluid (Fox et al., 2001) model of registration is used, in which the Green's function of the governing operator is spatially uniform and fixed. If the correlations are assumed to be long-range (i.e., the deformations are spatially quite smooth), there is more signal enhancement in large homogeneous regions such as the white matter, whereas if the correlations are assumed to be short-range (i.e., the deformations are spatially quite rough, as in the fluid registration model of Fox et al., 2001), there is typically more sensitivity to finer-scale differences (as found in the gray matter in the Fox et al. study), while sacrificing some power to detect broader-scale differences (e.g., the failure to detect white matter atrophy in Fox et al., 2001). In future, the differential sensitivity of both approaches could be combined by estimating these spatially varying correlations empirically from anatomical landmarks using 6-dimensional covariance

tensors (Fillard et al., 2008) and incorporating them into a statistically-based adaptive registration model as we have begun to do (Brun et al., 2007 and 2008).

In this paper, the correlations between atrophy and CSF biomarkers are also of significant interest. Prior literature has indicated that there is lower ABeta42, but higher tau and p-tau protein, in the CSF of AD patients versus those with other dementia subtypes or normal subjects (Andreasen et al. 2001; Itoh et al., 2001; Verbeek et al., 2003; Clark et al., 2003; Hampel et al., 2004). More recently, researchers have also investigated the utility of using these markers for predicting conversion from MCI to AD (Fagan et al., 2007; Li et al., 2007). In our results, progressive temporal lobe atrophy was highly correlated with baseline p-tau, tau/ABeta42 ratio (for both AD groups and all subjects pooled), ABeta42, and tau (the latter two only for data pooled across all diagnostic groups). This suggests that p-tau and tau/Abeta42 may be more clinically useful than Abeta42 or tau in predicting ongoing atrophy (in Fig. 4, CDF curves rise more rapidly for the correlations with p-tau and with the tau/ABeta42 ratio).

We could not demonstrate significant correlations between biomarkers and ongoing temporal lobe atrophy in the MCI group. This is perhaps not surprising due to the heterogeneous nature of MCI, and the relatively small sample of 40 subjects.

Clinical measures correlated more strongly with atrophy rates in MCI than in AD, supporting the use of serial neuropsychiatric testing in monitoring disease progression in MCI. In AD, atrophy rates exceeded those in MCI, but did not correlate so strongly with interval changes in neuropsychiatric test scores. This may suggest that (1) decline in cognition is more tightly linked with atrophy rates early in the illness, or (2) in late AD, atrophy rates may eventually plateau or slow down, which may disrupt any correlation between the absolute rate of tissue loss and further changes in cognition, or (3) correlations may only be detectable in samples that are larger and/or have a broader range of disease severity. Our AD sample was only half the size of our MCI sample, and was somewhat restricted in disease severity to reflect relatively mild AD; by contrast, in recent study of 52 subjects with mild-to-moderate AD (Ridha et al., 2008), there was a strong association between brain atrophy rate and MMSE decline (r=0.59, p<0.0001). In addition, there is some evidence that atrophy rates do not slow down as AD progresses; Chan et al. (2003) found that in 12 patients with mild dementia (MMSE=23), scanned from a presymptomatic stage through to moderately severe dementia, mean yearly loss of brain volume was 2.8% (95% CI: 2.3–3.3), but rose by 0.32% per year (0.15–0.50). In 39 healthy control subjects, Scahill et al. (2003) also found rates of atrophy accelerated nonlinearly with increasing age, with the most marked changes occurring after the age of 70.

To summarize, our results further support the value of serial MRI scanning, combined with quantitative nonlinear registration, for tracking disease progression in Alzheimer's and MCI. Our detailed 3D Jacobian maps, reflecting regional brain atrophy, correlated well with disease progression and conversion to AD, as well as with various biomarkers and clinical measures. Moreover, groups of MCI converters and non-converters were differentiated by measures of temporal lobe atrophy over time.

Lastly, instead of separating hippocampus in our analysis, it was included as part of the temporal lobe. Any TBM study is limited by the accuracy with which deformable registration can match anatomical boundaries between individual brains and corresponding regions on the template. Our mean deformation template (MDT) was created after rigorous nonlinear registration, and geometric centering. Most anatomical features and boundaries are well-preserved in the MDT, and the hippocampus is sufficiently discernible to be labeled by hand. Even so, it may not always be possible to achieve accurate regional measurements of atrophy in small regions such as the hippocampus, since that would require a locally highly accurate registration. Some research groups have successfully computed hippocampal atrophy rates

from fluid registration methods (e.g., Crum et al., 2001), and found that they can be superior to manual delineations in separating AD from controls ($p<0.0001$; Barnes et al., 2007a,b) and more reliable (van de Pol et al., 2007).

To detect more subtle effects, direct modeling of brain structures, e.g., using surface-based geometrical methods (e.g., Morra et al., 2008a,b), or using a template in conjunction with boundary shift integral measures (Barnes et al., 2007a,b), may offer additional statistical power to detect subregional differences. We are currently investigating longitudinal hippocampal changes using the ADNI dataset with a range of different methods, which we plan to report in the future.

Acknowledgments

The data used in preparing this article were obtained from the Alzheimer's Disease Neuroimaging Initiative database (www.loni.ucla.edu/ADNI). Many ADNI investigators therefore contributed to the design and implementation of ADNI or provided data but did not participate in the analysis or writing of this report. A complete listing of ADNI investigators is available at www.loni.ucla.edu/ADNI/Collaboration/ADNI_Citation.shtml. This work was primarily funded by the ADNI (principal investigator: Michael Weiner; NIH grant number U01 AG024904). ADNI is funded by the National Institute of Aging, the National Institute of Biomedical Imaging and Bioengineering (NIBIB), and the Foundation for the National Institutes of Health, through generous contributions from the following companies and organizations: Pfizer Inc., Wyeth Research, Bristol-Myers Squibb, Eli Lilly and Company, GlaxoSmithKline, Merck & Co. Inc., AstraZeneca AB, Novartis Pharmaceuticals Corporation, the Alzheimer's Association, Eisai Global Clinical Development, Elan Corporation plc, Forest Laboratories, and the Institute for the Study of Aging (ISOA), with participation from the U.S. Food and Drug Administration. The grantee organization is the Northern California Institute for Research and Education, and the study is coordinated by the Alzheimer's Disease Cooperative Study at the University of California, San Diego. Algorithm development for this study was also funded by the NIA, NIBIB, the National Library of Medicine, and the National Center for Research Resources (AG016570, EB01651, LM05639, RR019771 to PT). Author contributions were as follows: AL, IY, NP, XH, SL, AT, NS, and PT performed the image analyses; CJ, MAB, PB, JG, CW, BB, LS, JT, AF, DH, JK, GA, and MW contributed substantially to the image and data acquisition, study design, quality control, calibration and pre-processing, databasing and image analysis. We thank Anders Dale for his contributions to the image pre-processing and the ADNI project.

References

Aganj I, Sapiro G, Parikshak N, Madsen SK, Thompson PM. Measurement of cortical thickness from MRI by minimum line integrals on soft-classified tissue. 2008Submitted to Hum. Brain Mapp

Andreasen N, Minthon L, Davidsson P, et al. Evaluation of CSF-tau and CSF- Abeta$_{42}$ as diagnostic markers for Alzheimer disease in clinical practice. Arch Neurol 2001;58:373–379. [PubMed: 11255440]

Ashburner J, Friston KJ. Voxel-based morphometry — the methods. NeuroImage 2000 June;11(6):805–821. [PubMed: 10860804]

Ashburner, J.; Friston, KJ. Morphometry. In: Ashburner, J.; Friston, KJ.; Penny, W., editors. Human Brain Function. Academic Press; 2003.

Barnes J, Lewis EB, Scahill RI, Bartlett JW, Frost C, Schott JM, Rossor MN, Fox NC. Automated measurement of hippocampal atrophy using fluid-registered serial MRI in AD and controls. J Comput Assist Tomogr 2007a Jul–Aug;31(4):581–587. [PubMed: 17882036]

Barnes J, Boyes RG, Lewis EB, Schott JM, Frost C, Scahill RI, Fox NC. Automatic calculation of hippocampal atrophy rates using a hippocampal template and the boundary shift integral. Neurobiol Aging 2007b;28(11):1657–1663. [PubMed: 16934913]2007 Nov. Electronic Publication 2006 Aug 28

Barnes J, Bartlett JW, van de Pol LA, Loy CT, Scahill RI, Frost C, Thompson P, Fox NC. A meta-analysis of hippocampal atrophy rates in Alzheimer's disease. Neurobiol Aging. 2008 Mar 15;[Electronic Publication ahead of print]

Baron JC, Chetelat G, Desgranges B, Perchey G, Landeau B, de la Sayette V, Eustache F. In vivo mapping of gray matter loss with voxel-based morphometry in mild Alzheimer's disease. Neuroimage 2001;14:298–309. [PubMed: 11467904]

Bartzokis G, Cummings JL, Sultzer D, Henderson VW, Nuechterlein KH, Mintz J. White matter structural integrity in healthy aging adults and patients with Alzheimer disease: a magnetic resonance imaging study. Arch Neurol 2003;60 (3):393–398. [PubMed: 12633151]

Benjamini Y, Hochberg Y. Controlling the false discovery rate: a practical and powerful approach to multiple testing. J R Statist Soc B 1995;57 (1):289–300.

Boyes RG, Rueckert D, Aljabar P, Whitwell J, Schott JM, Hill DL, Fox NC. Cerebral atrophy measurements using Jacobian integration: comparison with the boundary shift integral. Neuroimage 2006 Aug 1;32(1):159–169. [PubMed: 16675272]Electronic Publication 2006 May 3

Braak H, Braak E. Neuropathological staging of Alzheimer-related changes. Acta Neuropathol (Berl) 1991;82:239–259. [PubMed: 1759558]

Brun CC, Lepore N, Pennec X, Chou YY, Lopez OL, Aizenstein HJ, Becker JT, Toga AW, Thompson PM. Comparison of Standard and Riemannian Elasticity for Tensor-Based Morphometry in HIV/AIDS, in MICCAI 2007. 2007accepted for the MICCAI Workshop on Image Registration, June 18 2007

Brun CC, Lepore N, Pennec X, Chou YY, Lee AD, McMahon KL, de Zubicaray GI, Meredith M, Wright MJ, Barysheva M, Toga AW, Thompson PM. A new registration method based on log–Euclidean tensor metrics and its application to genetic studies. 2008ISBI 2008, Feb. 2008

Bullmore ET, Suckling J, Overmeyer S, Rabe-Hesketh S, Taylor E, Brammer MJ. Global, voxel, and cluster tests, by theory and permutation, for a difference between two groups of structural MR images of the brain. IEEE Trans Med Imag 1999 Jan;18(1):32–42.

Choi SJ, Lim KO, Monteiro I, Reisberg B. Diffusion tensor imaging of frontal white matter microstructure in early Alzheimer's disease: a preliminary study. J Geriatr Psychiatry Neurol 2005;18:12–19. [PubMed: 15681623]

Clark CM, Xie S, Chittams J, Ewbank D, Peskind E, Galasko D, Morris JC, McKeel DW Jr, Farlow M, Weitlauf SL, Quinn J, Kaye J, Knopman D, Arai H, Doody RS, DeCarli C, Leight S, Lee VMY, Trojanowski JQ. Cerebrospinal fluid tau and beta-amyloid: how well do these biomarkers reflect autopsy-confirmed dementia diagnoses. Arch Neurol 2003;60:1696–1702. [PubMed: 14676043]

Cardenas VA, Studholme C, Gazdzinski S, Durazzo TC, Meyerhoff DJ. Deformation-based morphometry of brain changes in alcohol dependence and abstinence. Neuroimage 2007;34:879–887. [PubMed: 17127079]

Chan D, Janssen JC, Whitwell JL, Watt HC, Jenkins R, Frost C, Rossor MN, Fox NC. Change in rates of cerebral atrophy over time in early-onset Alzheimer's disease: longitudinal MRI study. Lancet 2003 Oct 4;362(9390):1121–1122. [PubMed: 14550701]

Chiang MC, Dutton RA, Hayashi KM, Lopez OL, Aizenstein HJ, Toga AW, Becker JT, Thompson PM. 3D pattern of brain atrophy in HIV/AIDS visualized using tensor-based morphometry. Neuroimage 2007a;34:44–60. [PubMed: 17035049]

Chiang MC, Reiss AL, Lee AD, Bellugi U, Galaburda AM, Korenberg JR, Mills DL, Toga AW, Thompson PM. 3D pattern of brain abnormalities in Williams syndrome visualized using tensor-based morphometry. Neuroimage 2007b;36:1096–1109. [PubMed: 17512756]

Christensen GE, Johnson HJ, Vannier MW. Synthesizing average 3D anatomical shapes. Neuroimage 2006;32:146–158. [PubMed: 16697223]

Chung MK, Worsley KJ, Paus T, Cherif C, Collins DL, Giedd JN, Rapoport JL, Evans AC. A unified statistical approach to deformation-based morphometry. Neuroimage 2001;14:595–606. [PubMed: 11506533]

Cockrell JR, Folstein MF. Mini-Mental State Examination (MMSE). Psychopharmacol Bull 1988;24:689–692. [PubMed: 3249771]

Collins DL, Neelin P, Peters TM, Evans AC. Automatic 3D intersubject registration of MR volumetric data in standardized Talairach space. J Comput Assist Tomogr 1994;18:192–205. [PubMed: 8126267]

Crum WR, Scahill RI, Fox NC. Automated hippocampal segmentation by regional fluid registration of serial MRI: validation and application in Alzheimer's disease. Neuroimage 2001 May;13(5):847–855. [PubMed: 11304081]

Davatzikos C, Genc A, Xu D, Resnick SM. Voxel-based morphometry using the RAVENS maps: methods and validation using simulated longitudinal atrophy. Neuroimage 2001;14:1361–1369. [PubMed: 11707092]

Edgington, ES. Randomization Tests. Vol. 3. Marcel Dekker; New York: 1995.

Fagan AM, Roe CM, Xiong C, Mintun MA, Morris JC, Holtzman DM. Cerebrospinal fluid tau/beta-amyloid$_{42}$ ratio as a prediction of cognitive decline in nondemented older adults. Arch Neurol 2007;64:343–349. [PubMed: 17210801]

Fillard P, Pennec X, Thompson PM, Ayache N. Evaluating brain anatomical correlations via Canonical correlation analysis on Sulcal lines. 2008To appear in NeuroImage

Folstein MF, Folstein SE, McHugh PR. "Mini-mental state". A practical method for grading the cognitive state of patients for the clinician. J Psychiatr Res 1975;12:189–198. [PubMed: 1202204]

Fox NC, Jenkins R, Leary SM, Stevenson VL, Losseff NA, Crum WR, Harvey RJ, Rossor MN, Miller DH, Thompson AJ. Progressive cerebral atrophy in MS: a serial study using registered, volumetric MRI. Neurology 2000;54(4):807–812. [PubMed: 10690967]2000 Feb 22

Fox NC, Crum WR, Scahill RI, Stevens JM, Janssen JC, Rossor MN. Imaging of onset and progression of Alzheimer's disease with voxel-compression mapping of serial magnetic resonance images. Lancet 2001;358:201–205. [PubMed: 11476837]

Freeborough PA, Fox NC. Modeling brain deformations in Alzheimer disease by fluid registration of serial 3D MR images. J Comput Assist Tomogr 1998;22:838–843. [PubMed: 9754126]

Frisoni GB, Laakso MP, Beltramello A, Geroldi C, Bianchetti A, Soininen H, Trabucchi M. Hippocampal and entorhinal cortex atrophy in frontotemporal dementia and Alzheimer's disease. Neurology 1999;52:91–100. [PubMed: 9921854]

Genovese CR, Lazar NA, Nichols T. Thresholding of statistical maps in functional neuroimaging using the false discovery rate. Neuroimage 2002;15:870–878. [PubMed: 11906227]

Good CD, Johnsrude IS, Ashburner J, Henson RN, Friston KJ, Frackowiak RS. A voxel-based morphometric study of ageing in 465 normal adult human brains. Neuroimage 2001;14:21–36. [PubMed: 11525331]

Hampel H, Buerger K, Zinkowski R, et al. Measurement of phosphorylated tau epitopes in the differential diagnosis of Alzheimer disease: a comparative cerebrospinal fluid study. Arch Gen Psychiatry 2004;61:95–102. [PubMed: 14706948]

Hua X, Leow A, Levitt J, Caplan R, Thompson P, Toga A. Detecting brain growth patterns in normal children using tensor-based morphometry. Hum Brain Mapp. 2007

Hua X, Leow AD, Parikshak N, Lee S, Chiang MC, Toga AW, Jack CR, Weiner MW, Thompson PM. The Alzheimer's Disease Neuroimaging Initiative. Tensor-based morphometry as a neuroimaging biomarker for Alzheimer's disease: an MRI study of 676 AD, MCI, and normal subjects. Neuroimage. 2008(Electornic Publication ahead of print)

Hughes CP, Berg L, Danziger WL, Coben LA, Martin RL. A new clinical scale for the staging of dementia. Br J Psychiatry 1982;140:566–572. [PubMed: 7104545]

Itoh N, Arai H, Urakami K, et al. Large-scale, multicenter study of cerebrospinal fluid tau protein phosphorylated at serine 199 for the antemortem diagnosis of Alzheimer's disease. Ann Neurol 2001;50:150–156. [PubMed: 11506396]

Jack C, Bernstein M, Fox N, Thompson P, Alexander G, Harvey D, Borowski B, Britson P, Whitwell J, Ward C, Dale A, Felmlee J, Gunter J, Hill D, Killiany R, Schuff N, Fox-Bosetti S, Lin C, Studholme C, DeCarli C, Krueger G, Ward H, Metzger G, Scott K, Mallozzi R, Blezek D, Levy J, Debbins J, Fleisher A, Albert M, Green R, Bartzokis G, Glover G, Mugler JI, Weiner M. The Alzheimer's Disease Neuroimaging Initiative (ADNI): the MR imaging protocol. J Magn Reson Imaging 2008;27(4):685–691. [PubMed: 18302232]2008 Apr

Joshi S, Davis B, Jomier M, Gerig G. Unbiased diffeomorphic atlas construction for computational anatomy. Neuroimage 2004;23 (Suppl 1):S151–S160. [PubMed: 15501084]

Jovicich J, Czanner S, Greve D, Haley E, van der Kouwe A, Gollub R, Kennedy D, Schmitt F, Brown G, Macfall J, Fischl B, Dale A. Reliability in multi-site structural MRI studies: effects of gradient non-linearity correction on phantom and human data. Neuroimage 2006;30:436–443. [PubMed: 16300968]

Kochunov P, Lancaster J, Thompson P, Toga AW, Brewer P, Hardies J, Fox P. An optimized individual target brain in the Talairach coordinate system. Neuroimage 2002;17:922–927. [PubMed: 12377166]

Kovacevic N, Henderson JT, Chan E, Lifshitz N, Bishop J, Evans AC, Henkelman RM, Chen XJ. A three-dimensional MRI atlas of the mouse brain with estimates of the average and variability. Cereb Cortex 2005;15:639–645. [PubMed: 15342433]

Lee VM, Trojanowski JQ. Progress from Alzheimer's tangles to pathological tau points towards more effective therapies now. J Alzheimers Dis 2006;9(3 Suppl):257–262. [PubMed: 16914864]Review

Leow, A.; Huang, SC.; Geng, A.; Becker, JT.; Davis, S.; Toga, AW.; Thompson, PM. Information Processing in Medical Imaging. Glenwood Springs; Colorado, USA: 2005a. Inverse consistent mapping in 3D deformable image registration: its construction and statistical properties; p. 493-503.

Leow, AD.; Thompson, PM.; Hayashi, KM.; Bearden, C.; Nicoletti, MA.; Monkul, SE.; Brambilla, P.; Sassi, RB.; Mallinger, AG.; Soares, JC. Lithium Effects on Human Brain Structure Mapped Using Longitudinal MRI. Society for Neuroscience; Washington, DC. 2005b.

Leow AD, Klunder AD, Jack CR Jr, Toga AW, Dale AM, Bernstein MA, Britson PJ, Gunter JL, Ward CP, Whitwell JL, Borowski BJ, Fleisher AS, Fox NC, Harvey D, Kornak J, Schuff N, Studholme C, Alexander GE, Weiner MW, Thompson PM. Longitudinal stability of MRI for mapping brain change using tensor-based morphometry. Neuroimage 2006;31:627–640. [PubMed: 16480900]

Leow A, Yanovsky I, Chiang M, Lee A, Klunder A, Lu A, Becker J, Davis S, Toga A, Thompson P. Statistical properties of Jacobian Maps and the realization of unbiased large-deformation nonlinear image registration. IEEE Trans Med Imag 2007;26 (6):822–832.

Lepore N, Brun C, Chou Y, Chiang M, Dutton R, Hayashi K, Lu A, Lopez O, Aizenstein H, Toga A, Becker J, Thompson P. Generalized tensor-based morphometry of HIV/AIDS using multivariate statistics on strain matrices and their application to HIV/AIDS. IEEE Transactions on Medical Imaging 2008;27 (1):129–141. [PubMed: 18270068]

Li G, Sokal I, Quinn JF, Leverenz JB, Brodey M, Schellenberg GD, Kaye JA, Raskind MA, Zhang J, Peskind ER, Montine TJ. CSF tau/Aβ_{42} ratio for increased risk of mild cognitive impairment. Neurology 2007;69:631–639. [PubMed: 17698783]

Lerch JP, Evans AC. Cortical thickness analysis examined through power analysis and a population simulation. NeuroImage 2005;24:163–173. [PubMed: 15588607]

Lorenzen P, Prastawa M, Davis B, Gerig G, Bullitt E, Joshi S. Multi-modal image set registration and atlas formation. Med Image Anal 2006;10:440–451. [PubMed: 15919231]

Lynch CA, Walsh C, Blanco A, Moran M, Coen RF, Walsh JB, Lawlor BA. The clinical dementia rating sum of box score in mild dementia. Dement Geriatr Cogn Disord 2006;21:40–43. [PubMed: 16254429]

Mazziotta J, Toga A, Evans A, Fox P, Lancaster J, Zilles K, Woods R, Paus T, Simpson G, Pike B, Holmes C, Collins L, Thompson P, MacDonald D, Iacoboni M, Schormann T, Amunts K, Palomero-Gallagher N, Geyer S, Parsons L, Narr K, Kabani N, Le Goualher G, Boomsma D, Cannon T, Kawashima R, Mazoyer B. A probabilistic atlas and reference system for the human brain: International Consortium for Brain Mapping (ICBM). Philos Trans R Soc Lond B Biol Sci 2001;356:1293–1322. [PubMed: 11545704]

McKhann G, Drachman D, Folstein M, Katzman R, Price D, Stadlan EM. Clinical diagnosis of Alzheimer's disease: report of the NINCDS-ADRDA Work Group under the auspices of Department of Health and Human Services Task Force on Alzheimer's Disease. Neurology 1984;34:939–944. [PubMed: 6610841]

Medina D, deToledo-Morrell L, Urresta F, Gabrieli I, Moseley M, Fleischman D, Bennett D, Leurgans S, Turner D, Stebbins G. White matter changes in cognitive impairment and AD: a diffusion tensor imaging study. Neurobiol Aging 2006;27:663–672. [PubMed: 16005548]

Morra J, Tu Z, Apostolova LG, Green AE, Avedissian C, Madsen SK, Parikshak N, Hua X, Toga AW, Jack CR, Schuff N, Weiner MW, Thompson PM. Automated 3D mapping of hippocampal atrophy and its clinical correlates in 400 subjects with Alzheimer's disease, mild cognitive impairment, and elderly controls, ISBI. 2008a

Morra, J.; Tu, Z.; Apostolova, LG.; Green, AE.; Avedissian, C.; Madsen, SK.; Parikshak, N.; Toga, AW.; Jack, CR.; Schuff, N.; Weiner, MW.; Thompson, PM. Automated mapping of hippocampal atrophy in 1-year repeat MRI data in 490 subjects with Alzheimer's disease, mild cognitive impairment, and

elderly controls, submitted to NeuroImage. In: Thompson, PM.; Miller, MI.; Poldrack, R.; Nichols, T., editors. Special Issue on Mathematics in Brain Imaging. 2008b. Sept. 14 2008

Morris JC. The Clinical Dementia Rating (CDR): current version and scoring rules. Neurology 1993;43:2412–2414. [PubMed: 8232972]

Mueller SG, Weiner MW, Thal LJ, Petersen RC, Jack C, Jagust W, Trojanowski JQ, Toga AW, Beckett L. The Alzheimer's disease neuroimaging initiative. Neuroimaging Clin N Am 2005a;15:869–877. xi–xii. [PubMed: 16443497]

Mueller SG, Weiner MW, Thal LJ, Petersen RC, Jack CR, Jagust W, Trojanowski JQ, Toga AW, Beckett L. Ways toward an early diagnosis in Alzheimer's disease: the Alzheimer's Disease Neuroimaging Initiative (ADNI). Alzheimers Dement 2005b;1:55–66. [PubMed: 17476317]

Nichols TE, Holmes AP. Nonparametric permutation tests for functional neuroimaging: a primer with examples. Hum Brain Mapp 2002;15:1–25. [PubMed: 11747097]

Paling SM, Williams ED, Barber R, Burton EJ, Crum WR, Fox NC, O'Brien JT. The application of serial MRI analysis techniques to the study of cerebral atrophy in late-onset dementia. Med Image Anal 2004 Mar;8(1):69–79. [PubMed: 14644147]

Petersen RC. Aging, mild cognitive impairment, and Alzheimer's disease. Neurol Clin 2000;18:789–806. [PubMed: 11072261]

Petersen RC, Smith GE, Waring SC, Ivnik RJ, Tangalos EG, Kokmen E. Mild cognitive impairment: clinical characterization and outcome. Arch Neurol 1999;56:303–308. [PubMed: 10190820]

Petersen RC, Doody R, Kurz A, Mohs RC, Morris JC, Rabins PV, Ritchie K, Rossor M, Thal L, Winblad B. Current concepts in mild cognitive impairment. Arch Neurol 2001;58:1985–1992. [PubMed: 11735772]

van de Pol LA, Barnes J, Scahill RI, Frost C, Lewis EB, Boyes RG, van Schijndel RA, Scheltens P, Fox NC, Barkhof F. Improved reliability of hippocampal atrophy rate measurement in mild cognitive impairment using fluid registration. Neuroimage 2007;34(3):1036–1041. [PubMed: 17174572]2007 Feb 1. Electronic Publication 2006 Dec 15

Riddle WR, Li R, Fitzpatrick JM, DonLevy SC, Dawant BM, Price RR. Characterizing changes in MR images with color-coded Jacobians. Magn Reson Imaging 2004;22:769–777. [PubMed: 15234445]

Ridha BH, Anderson VM, Barnes J, Boyes RG, Price SL, Rossor MN, Whitwell JL, Jenkins L, Black RS, Grundman M, Fox NC. Volumetric MRI and cognitive measures in Alzheimer disease: comparison of markers of progression. J Neurol. 20082008. Feb. 18.; [Electronic Publication ahead of print]

Rose SE, Chen F, Chalk JB, Zelaya F, Strugnell W, Benson M, Semple J, Doddrell D. Loss of connectivity in Alzheimer's disease: an evaluation of white matter tract integrity with colour coded diffusion tensor imaging. J Neurol Neurosurg Psychiatry 2000;69:528–530. [PubMed: 10990518]

Yoshiura T, Mihara F, Ogomori K, Tanaka A, Kaneko K, Masuda K. Diffusion tensor in posterior cingulate gyrus: correlation with cognitive decline in Alzheimer's disease. Neuroreport 2002;13:2299–2302. [PubMed: 12488815]

Scahill RI, Schott JM, Stevens JM, Rossor MN, Fox NC. Mapping the evolution of regional atrophy in Alzheimer's disease: unbiased analysis of fluid-registered serial MRI. Proc Natl Acad Sci U S A 2002;99(7):4703–4707. [PubMed: 11930016]2002 Apr 2

Scahill RI, Frost C, Jenkins R, Whitwell JL, Rossor MN, Fox NC. A longitudinal study of brain volume changes in normal aging using serial registered magnetic resonance imaging. Arch Neurol 2003;60 (7):989–994. [PubMed: 12873856]

Shattuck DW, Leahy RM. BrainSuite: an automated cortical surface identification tool. Med Image Anal 2002;6:129–142. [PubMed: 12045000]

Shaw LM, Korecka M, Clark CM, Lee VM-Y, Trojanowski JQ. Biomarkers of neurodegeneration for diagnosis and monitoring therapeutics. Nat Rev Drug Discov 2007;6:295–303. [PubMed: 17347655] (April 2007)

Sled JG, Zijdenbos AP, Evans AC. A nonparametric method for automatic correction of intensity nonuniformity in MRI data. IEEE Trans Med Imag 1998;17:87–97.

Storey JD. A direct approach to false discovery rates. J R Stat Soc B 2002;64 (Pt 3):479–498.

Studholme C, Cardenas V. A template free approach to volumetric spatial normalization of brain anatomy. Pattern Recogn Lett 2004;25:1191–1202.

Studholme C, Cardenas V. Population based analysis of directional information in serial deformation tensor morphometry. Med Image Comput Comput Assist Interv Int Conf Med Image Comput Comput Assist Interv 2007;10 (Pt 2):311–318. [PubMed: 18044583]

Studholme C, Cardenas V, Maudsley A, Weiner M. An intensity consistent filtering approach to the analysis of deformation tensor derived maps of brain shape. NeuroImage 2003;19 (4):1638–1649. [PubMed: 12948718]

Studholme C, Cardenas V, Blumenfeld R, Schuff N, Rosen HJ, Miller B, Weiner M. Deformation tensor morphometry of semantic dementia with quantitative validation. Neuroimage 2004;21:1387–1398. [PubMed: 15050564]

Studholme C, Drapaca C, Iordanova B, Cardenas V. Deformation-based mapping of volume change from serial brain MRI in the presence of local tissue contrast change. IEEE Trans Med Imag 2006;25(5): 626–639.2006 May

Thompson PM, Apostolova LG. Computational anatomical methods as applied to aging and dementia. Br J Radiol 2007 Dec;80(2):S78–91. [PubMed: 18445748]

Thompson PM, Giedd JN, Woods RP, MacDonald D, Evans AC, Toga AW. Growth patterns in the developing brain detected by using continuum mechanical tensor maps. Nature 2000;404:190–193. [PubMed: 10724172]

Thompson PM, Hayashi KM, de Zubicaray G, Janke AL, Rose SE, Semple J, Herman D, Hong MS, Dittmer SS, Doddrell DM, Toga AW. Dynamics of gray matter loss in Alzheimer's disease. J Neurosci 2003a;23:994–1005. [PubMed: 12574429]

Thompson PM, Hayashi KM, de Zubicaray G, Janke AL, Rose SE, Semple J, Herman D, Hong MS, Dittmer S, Doddrell DM, Toga AW. Dynamics of gray matter loss in Alzheimer's disease. J Neurosci 2003b;23(3):994–1005. [PubMed: 12574429]Feb. 1 2003

Thompson, PM.; Hayashi, KM.; Sowell, ER.; Gogtay, N.; Giedd, JN.; Rapoport, JL.; de Zubicaray, GI.; Janke, AL.; Rose, SE.; Semple, J.; Doddrell, DM.; Wang, YL.; van Erp, TGM.; Cannon, TD.; Toga, AW. Mapping cortical change in Alzheimer's disease, brain development, and schizophrenia, Special Issue on Mathematics in Brain Imaging. In: Thompson, PM.; Miller, MI.; Ratnanather, JT.; Poldrack, R.; Nichols, TE., editors. NeuroImage. Vol. 23. 2004. p. S2-S18.

Verbeek MM, De Jong D, Kremer HP. Brain-specific proteins in cerebrospinal fluid for the diagnosis of neurodegenerative diseases. Ann Clin Biochem 2003;40:25–40. [PubMed: 12542908]

Wechsler, D. Wechsler Memory Scale. Psychological Corp/Harcourt Brace Jovanovich; New York: 1987.

Whitwell JL, Schott JM, Lewis EB, MacManus DG, Fox NC. Using nine degrees-of-freedom registration to correct for changes in voxel size in serial MRI studies. Magn Reson Imaging 2004;22(7):993–999. [PubMed: 15288140]2004 Sep

Whitwell JL, Przybelski SA, Weigand SD, Knopman DS, Boeve BF, Petersen RC, Jack CR Jr. 3D maps from multiple MRI illustrate changing atrophy patterns as subjects progress from mild cognitive impairment to Alzheimer's disease. Brain 2007;130:1777–1786. [PubMed: 17533169]

Yanovsky, I.; Thompson, PM.; Klunder, AD.; Toga, AW.; Leow, AD. Local volume change maps in nonrigid registration: when are computed changes real?. International Conference on Medical Image Computing and Computer Assisted Intervention, Workshop on Statistical Registration; 2007. p. 1-8.

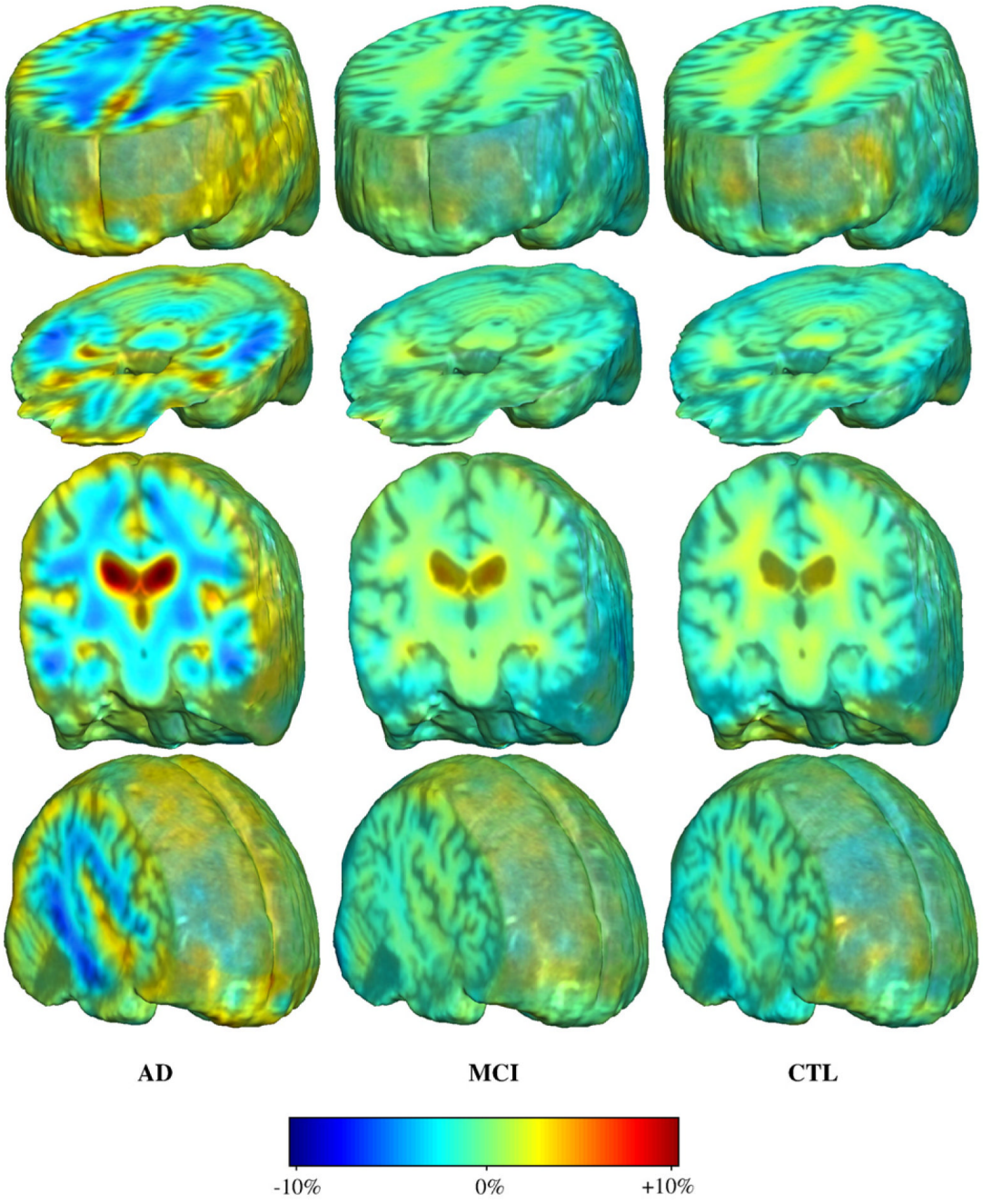

Fig. 1.

Unbiased registration was performed on 100 pairs of serial MR images, acquired 12 months apart, from the Alzheimer's Disease Neuroimaging Initiative (ADNI) dataset. The selected sample consisted of 20 patients with Alzheimer's disease (AD), 40 individuals with mild cognitive impairment (MCI), and 40 healthy elderly controls (CTL). The mean of the resulting Jacobian maps in each group is superimposed on a brain volume.

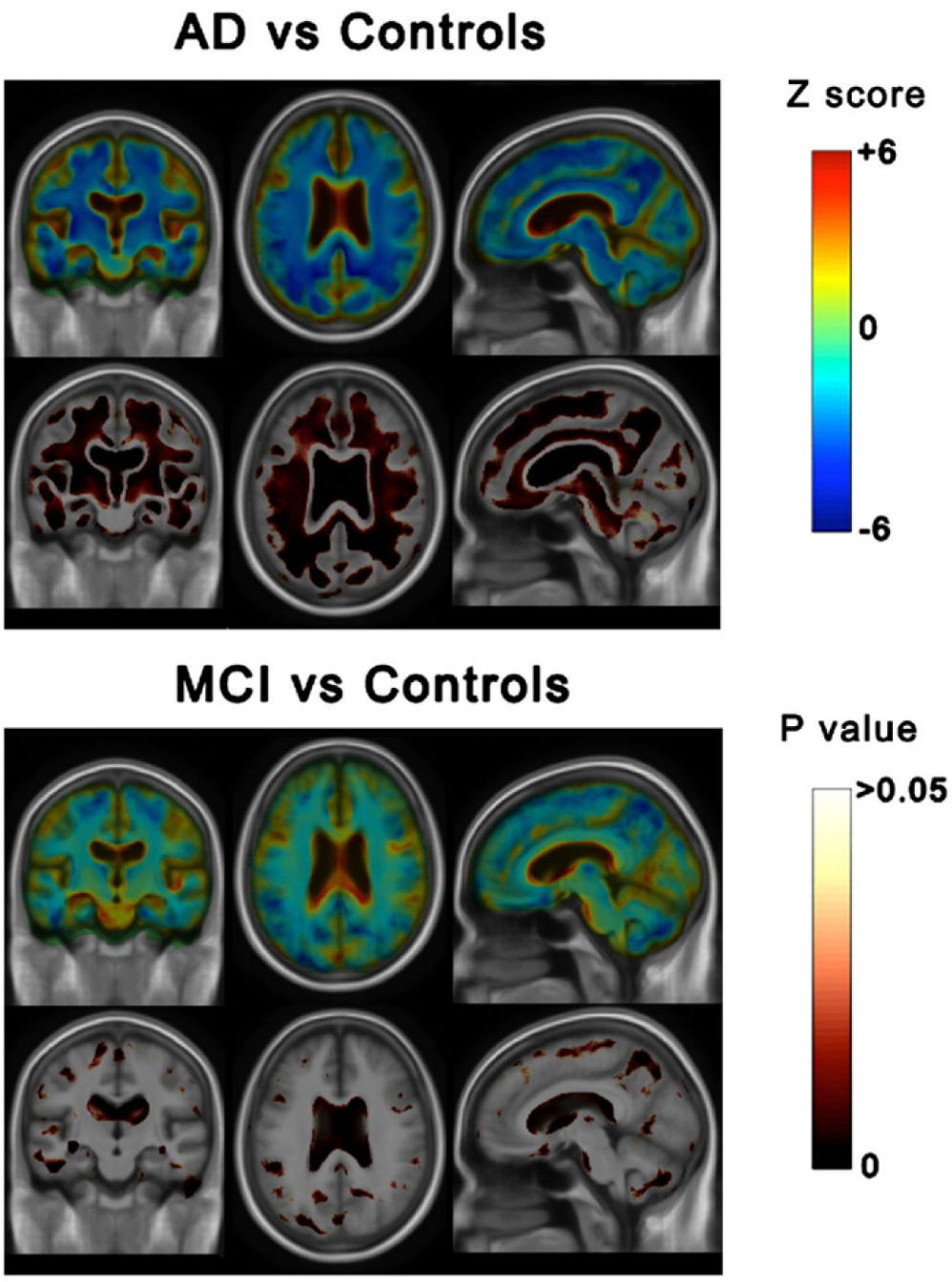

Fig. 2.

Voxel-wise Z-statistics (*top row*) comparing mean Jacobian values for AD (*N* =20) versus Controls (*N*=40) on the top, and MCI (*N*=40) versus Controls (*N*=40) on the bottom. Corresponding color-coded *P* maps also show the local significance of these differences (*bottom row*). There is widespread progressive atrophy in AD, at a faster mean rate than in normals — this difference in rates reaches the voxelwise significance level of 0.05 in most regions of the brain, and remains significant after corrected for multiple comparisons in ROIs including the temporal lobes, parietal lobes, occipital lobes, and frontal lobes. By contrast, for MCI versus Controls, only the parietal and temporal lobes reach ROI significance. Please refer to the Results section for more detailed discussions.

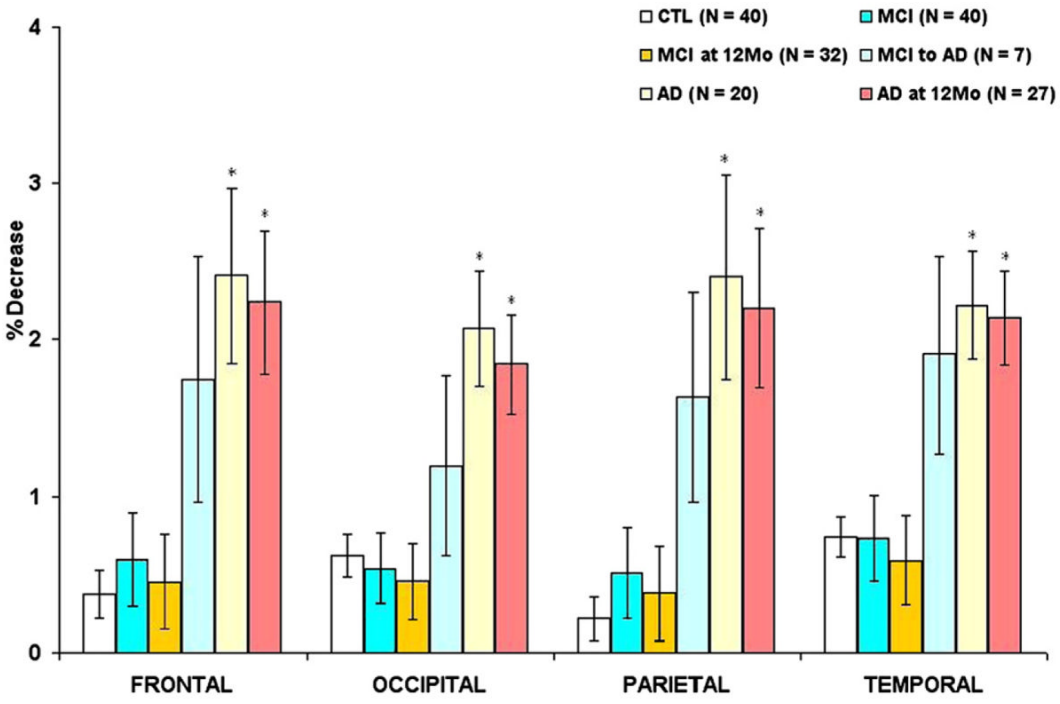

Fig. 3.

Percent brain tissue loss from baseline to follow-up as determined by the average Jacobian value within each lobe (with CSF excluded). The diagnosis for the AD, MCI, and CTL groups was determined at baseline. Here, *MCI at 12Mo* denotes subjects diagnosed with MCI at baseline who did not convert to AD at 12-month follow-up, whereas *MCI to AD* signifies those who had converted to AD at 12-month follow-up. One MCI subject's diagnosis converted back to control at follow-up, and thus was excluded from the MCI subgroups. The first bar in each group (colored *white*), shows mild but significant progressive atrophy in controls. The 2nd bar (*turquoise*) denotes MCI subjects at baseline, and is followed by bars denoting converters and non-converters. Mean rates are typically higher in the converters, comparable to subjects diagnosed as AD at both time-points, or AD at the last time point (*last two bars*). An * indicates $p<0.01$ for the comparison. Here, p values for MCI to AD group are not given, as there were only 7 subjects (significance levels were as follows: $p<0.01$ for all lobes in AD and AD at 12Mo; $p=0.012$, 0.054, and 0.02 in MCI for the temporal, frontal and occipital lobes; $p=0.02$ and 0.055 in controls for the occipital and temporal lobes; $p=0.068$ and 0.045 in MCI at 12Mo for occipital and temporal lobes; regions not reported here do not reach significance at the 0.05 level).

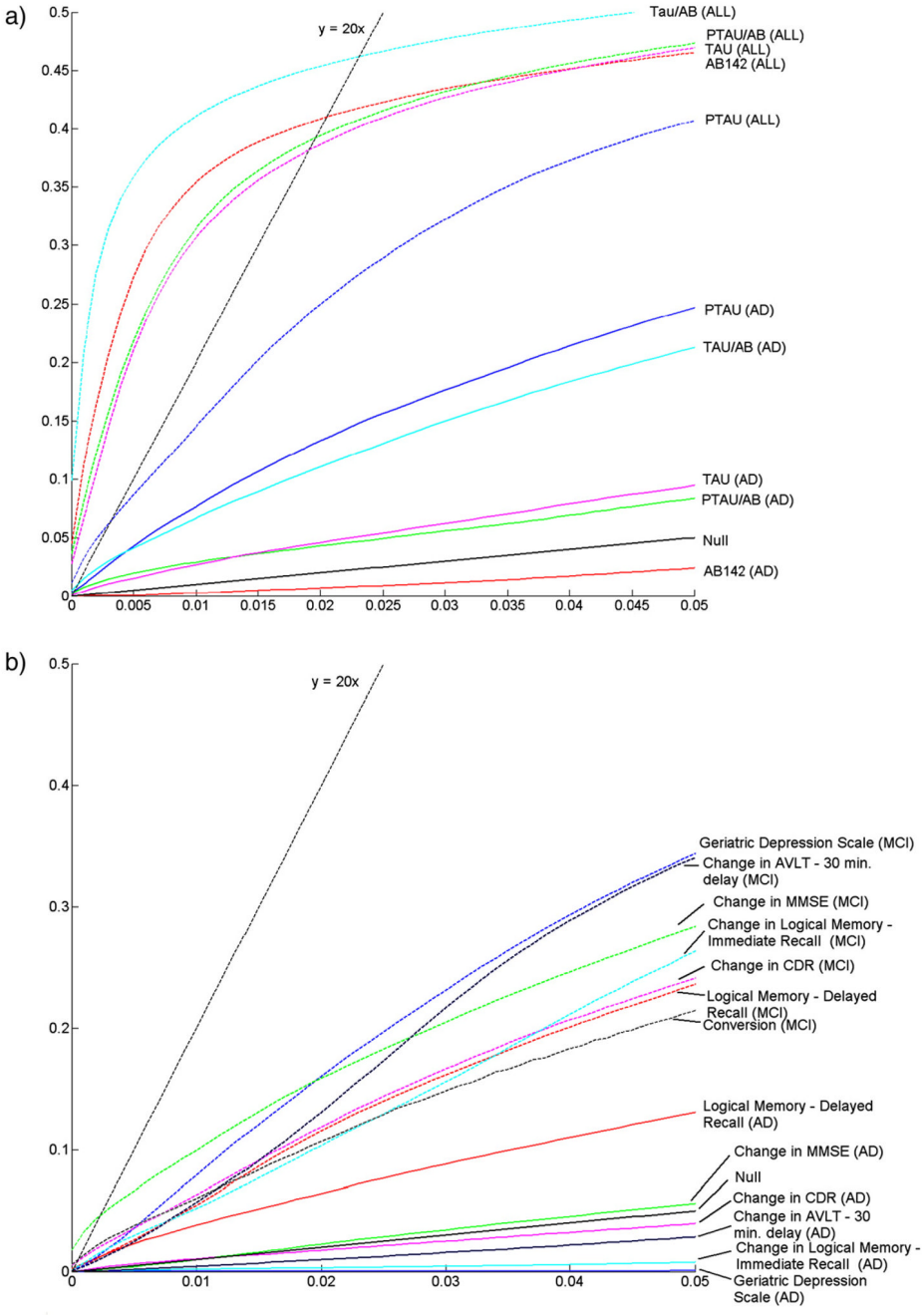

Fig. 4.

(a) CDF plots for voxel-wise correlation of progressive temporal lobe tissue loss in MCI, AD, and pooled groups (ALL, *N*=100) with (a) various biomarker indices including ABeta42 (AB142), tau protein (TAU), phosphorylated-tau 181 (PTAU), tau/ABeta42 ratio (TAUAB), and PTAU/AB42 ratio (PTAUAB), and (b) various clinical measures corresponding to those in Tables 1 and 2. Here, biomarkers correlate better in AD and the pooled group (but not in MCI), while clinical measures manifest better correlations in the MCI group. For more sensitive biomarkers or clinical measures, the departure of the early part of the corresponding CDF curve (i.e., the upswing) will be larger. The lack of significant correlations between biomarkers and ongoing temporal lobe atrophy in the MCI group is most likely due to the heterogeneous nature

of MCI. By contrast, the better correlations with clinical measures in the MCI group support the use of serial neuropsychiatric testing in monitoring disease progression. Please refer to text for more detailed discussions.

Table 1

Biomarker information and voxel-wise correlation results

	Relationship of ongoing temporal atrophy to biomarkers											
	Control			**MCI**			**AD**			**All pooled**		
	Mean (SD)	***N***	***p***	**Mean (SD)**	***N***	***p***	**Mean (SD)**	***N***	***p***	**Mean (SD)**	***N***	***p***
↓$A\beta_{1–42}$ (pg/mL)	210 (51)	26	0.6	154 (56)	26	0.3	129 (39)	14	0.6	171 (59)	66	0.001
↑Tau (pg/mL)	61 (22)	26	0.6	101 (58)	26	0.2	112 (40)	13	0.1	87 (48)	65	0.004
↑Tau/$A\beta_{1–42}$	0.31 (0.17)	26	0.5	0.81 (0.67)	26	0.7	0.92 (0.45)	13	0.1	0.63 (0.55)	65	0.0005
↑P-tau_{181P} (pg/mL)	24 (16)	26	0.3	32 (15)	26	0.5	39 (12)	14	0.03	30 (16)	66	0.02
↑P-tau_{181P}/$A\beta_{1–42}$	0.13 (0.12)	26	0.3	0.25 (0.17)	26	0.4	0.32 (0.15)	14	0.04	0.22 (0.16)	66	0.002

We give the standard deviations (SD) and the means of the underlying scores to give the reader an impression of the variables' distribution. A ↓ implies that *lower* numeric values of the variable are associated with greater atrophy, whereas a ↑ implies that *higher* numeric values of the variable are associated with greater atrophy.

Table 2

Baseline cognitive scores (a), changes in cognitive scores (b), and conversion from MCI to AD (c) and voxel-wise correlation results

	Relationship of ongoing temporal atrophy to:					
	a) Baseline cognitive scores					
	Control (*N*=40)		**MCI (*N*=40)**		**AD (*N*=20)**	
	Score quartile [25, 50, 75]	***p***	**Score quartile [25, 50, 75]**	***p***	**Score quartile [25, 50, 75]**	***p***
↓Logical memory — delayed	[10, 12, 14.5]	0.6	[5, 8, 9]	0.04	[3, 5, 6]	0.06
↑Geriatric Depression Score	[0, 1,1]	0.9	[1, 2, 2.25]	0.03	[1, 1.5, 2]	1
	b) Change in cognitive scores					
↓Change in MMSE	[−1, 0, 1]	0.6	[−2, 0, 1]	0.03	[−2, 0, 1]	0.3
↑Change in CDR	[0, 0, 0]	0.8	[0, 0, 0.125]	0.03	[0, 0, 0.125]	0.2
↓Change in logical memory — immediate	[−1, 2, 4]	0.9	[−3, −1, 2]	0.04	[−2, 0.5, 2]	0.7
↓Change in AVLT — 30 min delay	[−2, 1, 2]	0.5	[−1, 0, −1]	0.04	[−1, 0, 0.25]	0.5
	c) Conversion from baseline to follow-up					
MCI to AD (*N*=39)	—	—	*	0.03	—	—

We give the 25th, 50th, and 75th percentiles for these variables to give the reader an impression of their distribution. A ↓ implies that *lower* numeric values of the variable are associated with greater atrophy, whereas an ↑ implies that *higher* numeric values of the variable are associated with greater atrophy.

*Conversion was coded as 1 for converting (*N*=7), 0 for not converting (*N*=32).